Cerebral Cortex, April 2021;31: 1914–1926

doi: 10.1093/cercor/bhaa330
Advance Access Publication Date: 9 December 2020
Original Article

ORIGINAL ARTICLE

Temporal Dynamics and Neuronal Specificity of Grin3a Expression in the Mouse Forebrain

Alvaro Murillo[1,2], Ana I. Navarro[1], Eduardo Puelles[1], Yajun Zhang[3], Timothy J. Petros[3] and Isabel Pérez-Otaño[1]

[1]Instituto de Neurociencias, Consejo Superior de Investigaciones Científicas – Universidad Miguel Hernández, 03550 Sant Joan d'Alacant, Spain, [2]UK Dementia Research Institute at Cardiff University, CF24 4HQ Cardiff, UK and [3]Eunice Kennedy Shriver National Institute of Child Health and Human Development, Bethesda, MD, USA

Address correspondence to Isabel Pérez-Otaño, Instituto de Neurociencias, CSIC-UMH, Av. Ramón y Cajal s/n, 03550 Sant Joan d'Alacant, Spain. Email: otano@umh.es.

Abstract

GluN3A subunits endow N-Methyl-D-Aspartate receptors (NMDARs) with unique biophysical, trafficking, and signaling properties. GluN3A-NMDARs are typically expressed during postnatal development, when they are thought to gate the refinement of neural circuits by inhibiting synapse maturation, and stabilization. Recent work suggests that GluN3A also operates in adult brains to control a variety of behaviors, yet a full spatiotemporal characterization of GluN3A expression is lacking. Here, we conducted a systematic analysis of *Grin3a* (gene encoding mouse GluN3A) mRNA expression in the mouse brain by combining high-sensitivity colorimetric and fluorescence *in situ* hybridization with labeling for neuronal subtypes. We find that, while *Grin3a* mRNA expression peaks postnatally, significant levels are retained into adulthood in specific brain regions such as the amygdala, medial habenula, association cortices, and high-order thalamic nuclei. The time-course of emergence and down-regulation of *Grin3a* expression varies across brain region, cortical layer of residence, and sensory modality, in a pattern that correlates with previously reported hierarchical gradients of brain maturation and functional specialization. *Grin3a* is expressed in both excitatory and inhibitory neurons, with strong mRNA levels being a distinguishing feature of somatostatin interneurons. Our study provides a comprehensive map of *Grin3a* distribution across the murine lifespan and paves the way for dissecting the diverse functions of GluN3A in health and disease.

Key words: circuit refinement, excitatory glycine receptors, high-order thalamus, neocortical maturation, somatostatin interneurons

Introduction

N-Methyl-D-Aspartate receptors (NMDARs) are a family of excitatory glutamate-gated ion channels with central roles in brain plasticity, development, learning, and memory (Paoletti et al. 2013). Each receptor consists of four subunits, an obligatory GluN1 subunit and combinations of GluN2 (A-D) and GluN3 (A, B) subunits, which generates a variety of subtypes with distinct biophysical and signaling properties, distribution, and functions. Whereas GluN1 and GluN2 are expressed in the central nervous system throughout life in high concentrations, GluN3A subunits are rarer and predominate during early postnatal stages. Heteromeric complexes composed of GluN1/GluN2/GluN3A respond to glutamate and NMDA, and are thus bona-fide NMDARs. However, they have nonconventional properties that distinguish them from classical NMDARs (GluN1/GluN2 heteromers) including lower calcium permeability, reduced voltage-dependent block by magnesium, and lesser attachment to postsynaptic densities. Because of these properties, they can work as dominant-negative regulators of NMDAR-mediated

plasticity and have been proposed to fine-tune the refinement of neural circuits during critical postnatal periods by inhibiting the stabilization of nonused synapses and promoting their pruning (Pachernegg et al. 2012; Perez-Otano et al. 2016).

Recent studies point towards broader roles of GluN3A subunits in the mammalian brain. First, GluN3A can form GluN1/GluN3 complexes that do not bind glutamate and instead generate excitatory currents activated by glycine (Perez-Otano et al. 2001; Chatterton et al. 2002). Although initially studied in recombinant systems, native GluN1/GluN3A receptors have now been identified in juvenile mouse hippocampus and adult medial habenula (Grand et al. 2018; Otsu et al. 2019). Rather than modulating plasticity, their activation potentiates basal firing rates and could have a major influence on neuronal excitability. Second, while GluN3A protein and mRNA levels are largely down-regulated after critical developmental periods, the Allen Brain Atlas documents remaining *Grin3a* mRNA expression in adult brains and a variety of phenotypes of cognition, social, and aversive behavior have been reported in adult mice lacking GluN3A, suggesting that functional relevance may continue throughout life (Mohamad et al. 2013; Lee et al. 2016; Otsu et al. 2019). Third, genetic mutations or alterations in human *GRIN3A* expression have been linked to disorders of cognition, mood, and emotion such as schizophrenia, bipolar disorder, or substance abuse, suggesting alterations in the control of affective, impulsive traits or executive functions (Mueller and Meador-Woodruff 2004; Yang et al. 2015; Lee et al. 2016; Huang et al. 2017). Importantly, preclinical mouse studies provided causal relationships between age-inappropriate reactivation of functional GluN3A expression and pathological spine pruning in Huntington's disease, or maladaptive forms of plasticity that predispose to drug relapse (Marco et al. 2013, 2018; Yuan et al. 2013), making GluN3A an attractive candidate for therapeutic intervention.

At present it is unclear how GluN3A subunits subserve such diverse functions and whether links to behavior or disease endophenotypes reflect adult roles of GluN3A or faults in the developmental trajectories of specific neuronal circuits. A limitation for dissecting GluN3A functions has been the lack of a comprehensive understanding of the timing and regional variations in GluN3A expression throughout development and in the adult brain, and of the cellular populations where GluN3A is expressed. To address this limitation, we have conducted a systematic analysis of *Grin3a* mRNA expression in the mouse brain from embryonic to early postnatal and adult stages using colorimetric and fluorescence *in situ* hybridization (ISH). We find that, while subject to a prominent down-regulation, substantial *Grin3a* expression is retained in a subset of brain regions. Specifically, adult *Grin3a* expression was highest in multimodal or associative areas such as the insular, prefrontal, and anterior cingulate cortices or the claustrum, and in areas encoding or integrating internal emotional or arousal/awareness states such as the amygdala, medial habenula, or "high-order" thalamic nuclei. Throughout postnatal development, *Grin3a* expression exhibits precise temporal dynamics that differ in neocortical areas across sensory modalities and cortical layer. At the cellular level, *Grin3a* is expressed by both excitatory and inhibitory neurons, with high expression a distinguishing feature of somatostatin (Sst) interneurons.

Materials and Methods

Animals and Tissue Collection

Several strains of C57BL/6 J background mice were used: WT, GAD67^{GFP} (B6.Cg-Tg(Gad1-EGFP) (Tamamaki et al. 2003) and Nkx2.1-Cre::Ai9^{tdTomato}. The latter was obtained crossing Tg(Nkx2.1-Cre)2S and/J (JAX 008661; (Xu et al. 2008) and Ai9(B6.Cg-Gt(ROSA)26Sortm9(CAG-tdTomato)Hze/J (JAX 007909) (Madisen et al. 2010). Mice were housed 4–6 per cage with *ad libitum* access to food and water and maintained in a temperature-controlled environment on a 12-h light/dark cycle at humidity between 40 and 60% in a standard pathogen free environment. All procedures were conducted in accordance with the European and Spanish regulations (2010/63/UE; RD53/2013) and were approved by the Ethical Committee of the Government of the Generalitat Valenciana (2017/VSC/PEA/00196).

After deep anesthesia with isoflurane, mice were transcardially perfused with 4% paraformaldehyde in phosphate buffered saline (PBS) pH 7.4. Brains were removed and postfixed overnight at 4°C. From this step on, tissue treatment was different depending on the later technique. For colorimetric and fluorescence ISH, brains were then embedded in 4% agarose, sectioned coronally in 100 or 80 µm-thick slices respectively with a vibrating microtome and stored in PBS at 4°C. For RNAscope assays, tissue was immersed in 30% sucrose at 4°C and frozen in OCT. Frozen brains were sectioned at 14 µm with a cryostat and stored at –80°C.

Cloning and *In Situ* Hybridization

Templates for synthesizing *Grin3a* riboprobes were obtained by PCR from cDNA libraries of hippocampus of C57BL/6 using the following primers: forward GAACACATAGTGTACAGACTGC; reverse CTAGGATTCACAAGTCCGGTT. The resulting amplicon was purified with QIAquick gel extraction kit- (QIAGEN) and cloned into pBlueScript SK plasmid. Plasmids for riboprobes against *Gad1* mRNA were a gift from Dr Jordi Guimer. The riboprobes were: *Grin3a*-ctd (spanning 495 bp of the C-terminal domain, accession number NM_001033351.2) and *Gad1* (bp 934–1786 of the *Gad1* cDNA, accession number NM_008077). Plasmids were linearized and riboprobes labeled with UTP-digoxigenin or UTP-fluorescein during *in vitro* transcription using polymerase T3 or T7 (for antisense and sense riboprobes, respectively). Riboprobes were then purified by RNeasy Mini Kit Qiagen and concentrations measured with NanoDrop.

Free-floating 100 µm-thick brain sections were permeabilized with detergent mix (1% NP-40, 1% SDS, 0.5% sodium deoxycholate, 50 mM Tris pH 8.0, 1 mM EDTA, and 150 mM NaCl) for 1 h at room temperature, and incubated with digoxigenin-labeled riboprobes at 63°C in hybridization buffer (50% formamide; 2x saline-sodium citrate pH 5.3; 50 µg/mL heparin; 50 µg/mL tRNA; 50 µg/mL salmon sperm DNA; 0.1% Tween-20) overnight. Hybridized probes were detected using an alkaline phosphatase-conjugated antidigoxigenin (Roche 11 093 274 910, 1:2000) in blocking solution (2% Roche Blocking reagent and 20% sheep serum in MABT buffer) overnight at 4°C, followed by several washes in MABT buffer (500 mM maleic acid, 750 mM NaCl, 0.95 M NaOH, and 0.1% Tween-20, pH 7.5). For visualization, sections were then incubated at room temperature during 6 or 22 h in a solution containing

nitroblue tetrazolium chloride (NBT) and 5-bromo-4-chloro-3′-indolyphosphate p-toluidine salt (BCIP) in NTMT buffer (100 mM NaCl; 100 mM Tris-HCl pH 9.5; 50 mM MgCl2; 1% Tween-20) that produces a colored precipitate due to the reaction with alkaline phosphatase. After several washes in PBS 1x, sections were mounted onto Superfrost Plus slides (Thermo Fisher Scientific™), dehydrated, and coverslipped with DPX mounting solution.

Fluorescence *In Situ* Hybridization

Identical protocol to the described above was followed, except 80 µm-thick brain sections were used. Sections were incubated with digoxigenin- and fluorescein-labeled riboprobes (against *Grin3a* and *Gad1* mRNA, respectively) in hybridization buffer, followed by incubation with peroxidase-conjugated antidigoxigenin or antifluorescein antibodies (Roche 11 207 733 910; Roche 11 426 346 910, 1:2000). A TSA plus fluorescence kit was used for signal amplification and detection according to the manufacturer protocol (Thermo Fisher, NEL744001KT). To avoid nonspecific signal, endogenous peroxidases were inactivated by incubation with MABT-1% H_2O_2 for 1 h in the dark. Sense probes used as control yielded no signal. Double fluorescence ISH was performed with dual hybridization and duplication of detection and amplification steps. Sections were counterstained with DAPI, mounted onto Superfrost Plus slides (Thermo Fisher), air-dried, and cover-slipped with fluorescence mounting medium (DAKO).

Immunohistochemistry

After the fluorescence ISH procedure, free-floating brain sections were incubated with primary antibody in 1% BSA, 0.1% Triton X-100, and 1% NS in PBS overnight at 4°C. The following primary antibodies were used: rabbit anti-GFP (Synaptic systems 132 002, 1:1000), rabbit anti-Cux1 (Santa Cruz Biotechnology Sc-13 024, 1:500) and rat anti-Ctip2 (Abcam Ab18465, 1:500). After washing with PBS, sections were incubated with fluorophore-conjugated secondary antibody in 1% BSA, 0.1% Triton X-100 in PBS for 1 h at room temperature. The following secondary antibodies were used: anti-rabbit-Cy3 (Jackson Immunoresearch 111 175 144, 1:500), anti-rat-488 (Invitrogen A11006, 1:500) and anti-rabbit-488 (Invitrogen A11008, 1:500). After several washes in PBS, sections were counterstained with DAPI, mounted onto Superfrost Plus slides, air-dried, and coverslipped with fluorescence mounting medium (DAKO).

Image Acquisition and Analysis

Bright field images were acquired using a Leica DM6000B microscope with 5X and 10X objectives or a MZ16FA stereomicroscope equipped with a DC500 digital camera, and processed with Leica AF6000 software. Quantification of *Grin3a* expression across cortical layers and sensory modalities was performed using Fiji for automatic detection of positive labeling after background subtraction. Fluorescence confocal images were captured on an Olympus FV1200 with a 20X objective or a ZEISS AxioImager M2 microscope with an Apochromat 20X objective, and processed with FV10-ASW_Viewer and Zen Blue software, respectively. The colocalization of *Grin3a*-positive cells with neuronal subtype-specific markers was quantified using Fiji software.

For anatomical analysis, identification of structures and functional interpretation, the Mouse brain in stereotaxic coordinates (Paxinos and Franklin, 2019 Edition), the Mouse nervous system (Watson, Paxinos, Puelles, 2012 Edition) and the Atlas of the developing mouse brain (Paxinos, Halliday, Watson, Koutcherov, Wang, 2007 Edition) were used.

RNAscope *In Situ* Hybridization Assay

RNAscope® Multiplex Fluorescent Kit v2 (Advanced Cell Diagnostics) was used to perform ISH with the following probes: *Grin3A*-C1 (#551371), *Gad1*-C2 (#400951-C2), Slc17a7-C3 (*vGlut1*)(#416 631-C3), *Sst*-C3 (#404631-C3), and *tdTomato*-C2 (#317041-C2).

Briefly, slides were dried for 60 min at –20°C, washed in PBS for 5 min, then baked for 10 min at 60°C. The slides were postfixed by immersing them in prechilled 4% PFA for 10 min at ice, followed by two rinses in diH_2O. Slides were dehydrated for 5 min each in 50%, 70%, and 100% ethanol, then dried for 5 min at RT. About 5–8 drops of RNAscope hydrogen peroxide was applied to the slides for 10 min followed by diH_2O washing. Then, slides were transferred to a container with RNAscope target retrieval reagent and incubated at >95°C for 5 min, then incubated in 100% alcohol for 3 min. After drying the slides at RT, they were treated with Protease III for 20 min at 40°C. After rinsing two times in distilled water, 1X target probe mixes were applied to the brain sections and incubated at 40°C for 2 h in the HybEZ™ oven (Advanced Cell Diagnostics). Sections were then incubated with preamplifier and amplifier probes and develop HRP-C1, C2, and C3 signals with TSA Plus fluorophores (PerkinElmer) by following the RNAscope® Multiplex Fluorescent Kit v2 user manual. After washing, sections were stained for 30 s with DAPI.

Statistical Analysis

Statistical analysis was performed using GraphPad Prism 7. For qualitative and semi-quantitative analysis of colorimetric ISH data in Figures 1–4 and Supplementary Table 1, the following number of mice were analyzed: E17.5 ($n = 3$), P0 ($n = 6$), P3 ($n = 8$), P6 ($n = 16$, short and long exposure), P9 ($n = 6$), P12 ($n = 4$), adult ($n = 3$, long exposure). Two-way ANOVA followed by Bonferroni's multiple comparisons posthoc test was used to assess differences between groups in Figure 5D. In all figures, data are presented as means ± SEM.

Results

Predominant Postnatal *Grin3a* mRNA Expression and Down-Regulation into Adulthood

We began by comparing the relative levels and regional patterns of *Grin3a* mRNA expression in young (postnatal day (P) 6) and adult (3–4 months) mouse brains using colorimetric ISH. Here and for most other experiments, sections were processed using two different exposures to the developing solution. This allowed us to achieve the high sensitivity needed for detecting adult expression (22 h, high exposure, Fig. 1), while preserving a dynamic range for semi-quantitative assessment of expression levels at earlier postnatal stages (6 h, low exposure, Figs 2–4). P6 was chosen based on previous quantitative immunoblot analyses in rodent brain that reported maximal *Grin3a* expression over the P5–P9 time window (Al-Hallaq et al. 2002; Wong et al. 2002; Roberts et al. 2009).

A first inspection confirmed that highest *Grin3a* mRNA levels are found postnatally and decline dramatically in most brain regions into adulthood (Fig. 1). However, there were

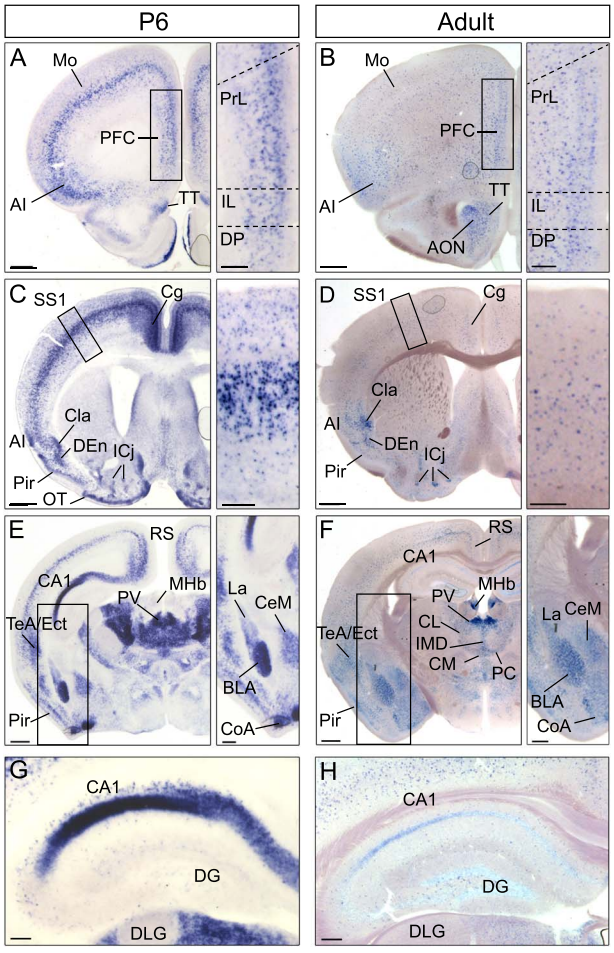

Figure 1. *Grin3a* expression is down-regulated into adulthood. Colorimetric ISH showing *Grin3a* mRNA expression in young (postnatal day (P)6; *A*, *C*, *E*, *G*) and adult mouse brain (*B*, *D*, *F*, *H*). Sections were exposed for 22 h to the developing solution to enhance sensitivity. Representative coronal sections at different rostro-caudal levels are displayed, and higher magnification images of the boxed areas are shown on the right. AI, agranular insular cortex; AON, anterior olfactory nucleus; BLA, basolateral amygdala; CA1, Cornu Ammonis 1; CeM, central amygdala; Cg, cingulate cortex; CL, centrolateral thalamic nucleus; Cla, claustrum; CM, centromedial thalamic nucleus; CoA, cortical amygdala; DEn, dorsal endopiriform nucleus; DG, dentate gyrus; DLG, dorsal lateral geniculate nucleus; DP, dorsal peduncular cortex; Ect, ectorhinal cortex; ICj, islands of Calleja; IL, infralimbic cortex; IMD, intermediodorsal thalamic nucleus; La, lateral amygdala; MHb, medial habenula nucleus; Mo, motor cortex; OT, olfactory tubercule; PC, paracentral thalamic nucleus, PFC, prefrontal cortex; Pir, piriform cortex; PrL, prelimbic cortex; PV, paraventricular thalamic nucleus; RS, retrosplenial cortex; SS1, somatosensory cortex 1; TeA, temporal association cortex; TT, tenia tecta. Scale bars: 500 µm (*A*-*F*); 200 µm (*G*-*H* and insets).

notable exceptions. Substantial *Grin3a* levels were retained in specific cortical areas including the prefrontal cortex (limbic and infralimbic divisions), anterior cingulate, retrosplenial, agranular insular, temporal association, ectorhinal, and perirhinal cortices (Fig. 1*B*, *D*, *F*, see Supplementary Fig. 1). This adult pattern of *Grin3a* expression correlates with a cortical hierarchy of functional specialization established based on connectivity patterns or structural properties (Fulcher et al. 2019; Harris et al. 2019). High adult levels of *Grin3a* mRNA were also observed in areas of the olfactory cortex (tenia tecta, anterior olfactory nucleus, dorsoendopiriform nucleus, islands of Calleja), in nuclei of the contiguous cortical or olfactory amygdala (anterior, ACo; and posteromedial, PMCo); and in basolateral and central amygdala (Fig. 1*B*, *D*, *F*, see Supplementary Fig. 1). Adult expression in the thalamus was lower and more restricted than at P6, but high levels were retained in some of the so-called "high-order" thalamic nuclei including midline (paraventricular, intermediodorsal, reuniens, rhomboid) and intralaminar nuclei (centromedial, paracentral, centrolateral) (Fig. 1*F*, see Supplementary Fig. 1). It is worth noting the exception of the medial habenula that displayed an opposite pattern of *Grin3a* expression, with high adult levels but low expression in young brains (Fig. 1*E* vs. *F*).

Our comparative analysis additionally revealed a clear dorsoventral gradient of *Grin3a* expression in principal neurons of adult CA1 hippocampus (see Supplementary Fig. 2). At P6, *Grin3a* was highly expressed in CA1 pyramidal neurons throughout the entire rostrocaudal extent of the hippocampus in both dorsal and ventral divisions (Fig. 1*G*, see Supplementary Fig. 2*A*, *B*, *D*, *E*). In contrast, expression in dorsal CA1 was virtually absent in adults but high levels were retained in ventral CA1 pyramidal neurons (Fig. 1*H*, see Supplementary Fig. 2*C* vs. *F*). As previously reported (Sucher et al. 1995), no expression was detected in CA2, CA3, or dentate gyrus at either age. However, we noted a previously unappreciated strong *Grin3a* mRNA signal in a small subset of neurons in the CA1 stratum oriens which was most prominent at P6 (see Supplementary Fig. 2, insets).

As introduced above, shorter exposure to the developing solution allowed a semi-quantitative analysis of postnatal *Grin3a* expression levels across the rostro-caudal brain axis (Fig. 2 and see Supplementary Table 1). The analysis revealed a unique pattern of *Grin3a* expression with several remarkable features. First, high *Grin3a* levels were observed in most neocortical areas with predominance in deeper layers at P6 (Fig. 2*A*-*H*, see extended laminar analysis below). Expression was also high throughout the entire rostro-caudal axis of the olfactory cortex including the rostral anterior olfactory nucleus and tenia tecta, the dorsal endopiriform nucleus and piriform cortex (Fig. 2*B*-*H*); in ACo and PMCo nuclei of the cortical amygdala (Fig. 2*E*-*H*); and in the interposed cortex amygdala transition zone (Fig. 2*F*, *G*). Second, high levels were found in the basolateral, basomedial, and basoposterior divisions of the amygdala. Lower but significant levels were detected in central and lateral amygdala (Fig. 2*F*, *G*, *H*). Third, *Grin3a* expression was especially strong in the thalamus where it prevailed in high-order thalamic nuclei including midline thalamic nuclei (paraventricular, reuniens, rhomboid), intralaminar, mediodorsal, posterior, and lateroposterior nucleus (analogous to the primate pulvinar). By contrast, *Grin3a* was absent or expressed at very low levels in first-order, primary sensory thalamic nuclei including the dorsolateral geniculate, ventral division of the medial geniculate, or ventral posterior nuclei (Fig. 2*D*-*H*).

Emergence and Down-regulation of *Grin3a* Expression Vary Across Brain Areas

While maximal *Grin3a* expression was previously reported in P6–P9 brains and assumed to homogeneously decline across brain regions into adulthood, earlier embryonic expression has been reported in human brains (Eriksson et al. 2002; Mueller and Meador-Woodruff 2003). Furthermore, GluN3A-NMDARs have been shown to control the propensity for precisely timed

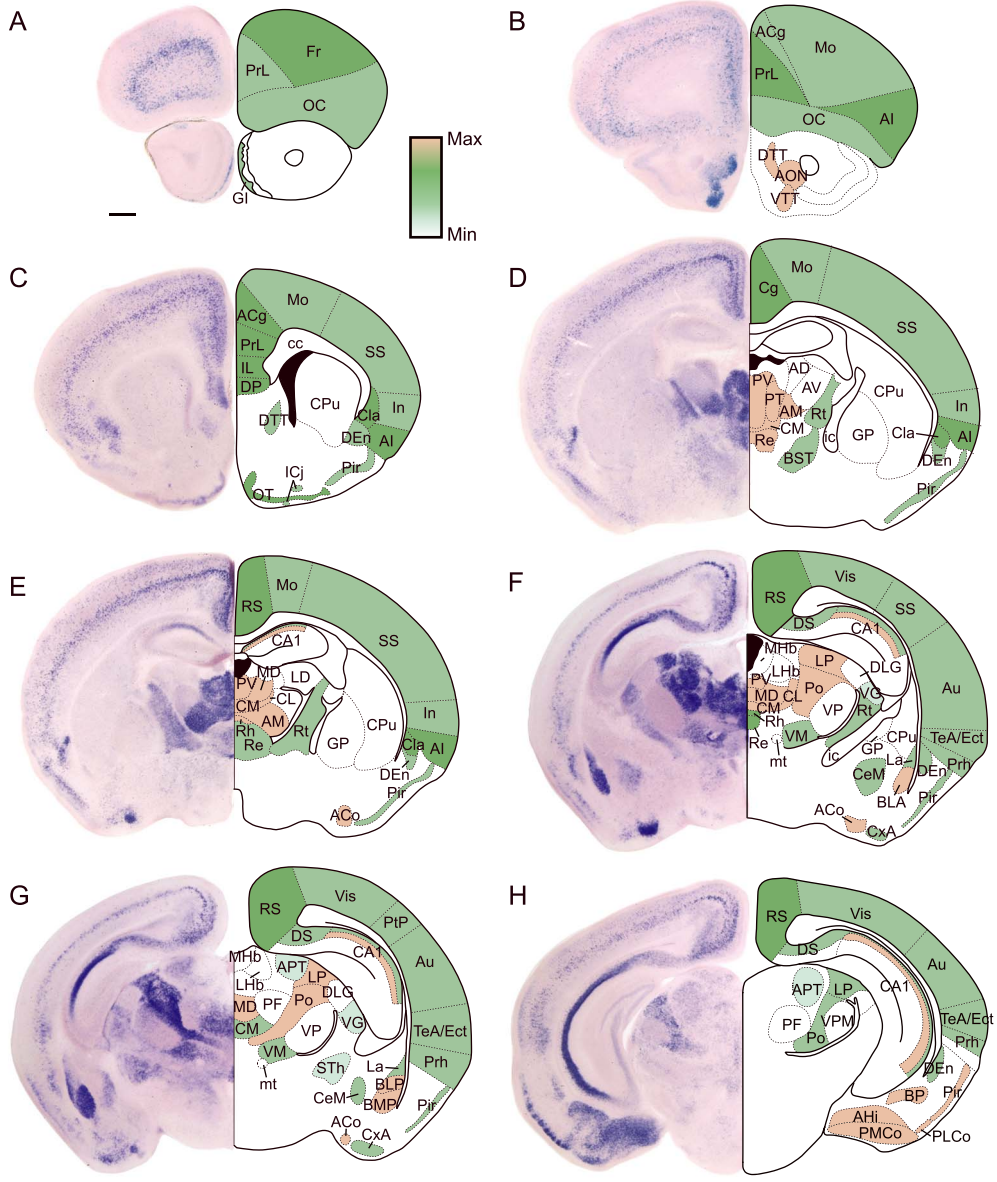

Figure 2. Regional distribution of *Grin3a* expression in early postnatal development. (*A-H*) Representative images of colorimetric ISH for *Grin3a* mRNA in coronal sections from P6 to P9 mouse brains. Here and in Figures 2–4, sections were exposed for 6 h to the developing solution. Corresponding schemes modified from the Paxinos's Atlas of the developing mouse brain are shown in the right, and mRNA expression levels are color-coded as indicated in the heatmap. The images were acquired at different rostro-caudal levels. Abbreviations are listed in Supplementary Table 1. Scale bars: 500 µm.

forms of cortical plasticity such as the developmental onset of long-term potentiation in the hippocampus (Roberts et al. 2009) or spike-timing dependent long-term depression in visual cortex (Larsen et al. 2014) and could be predicted to display a precise timing in specific brain regions. We thus investigated the developmental time-course of *Grin3a* expression from embryonic mouse brain through multiple stages of postnatal development (P0, P3, P6, P9, P12).

We found that the age of emergence and down-regulation of *Grin3a* expression varies significantly across brain regions. By embryonic day (E) 17.5, high levels of *Grin3a* mRNA were detected in the thalamus following a similar pattern to the observed postnatally, that is, absent/low in sensory thalamus but abundant in high-order nuclei (Fig 3C-E). *Grin3a* was also expressed at this early time-point in the CA1 hippocampus, amygdala, cortical amygdala (Fig. 3C-E), and in the claustrum (Fig. 3B), a nucleus highly interconnected with nearly all cortical areas and involved in multimodal sensory processing (Kim et al. 2016).

Grin3a expression in the neocortex was low at E17.5 (Fig. 3A-E), increased postnatally, and down-regulated by P12 (Fig. 4). Yet again differences in the timing of expression were noted across neocortical areas. *Grin3a* expression appeared earliest (by P0) in cingulate, retrosplenial, and piriform cortices (Fig. 4F, K, P). By P3, expression was observed in most of the neocortex including prefrontal

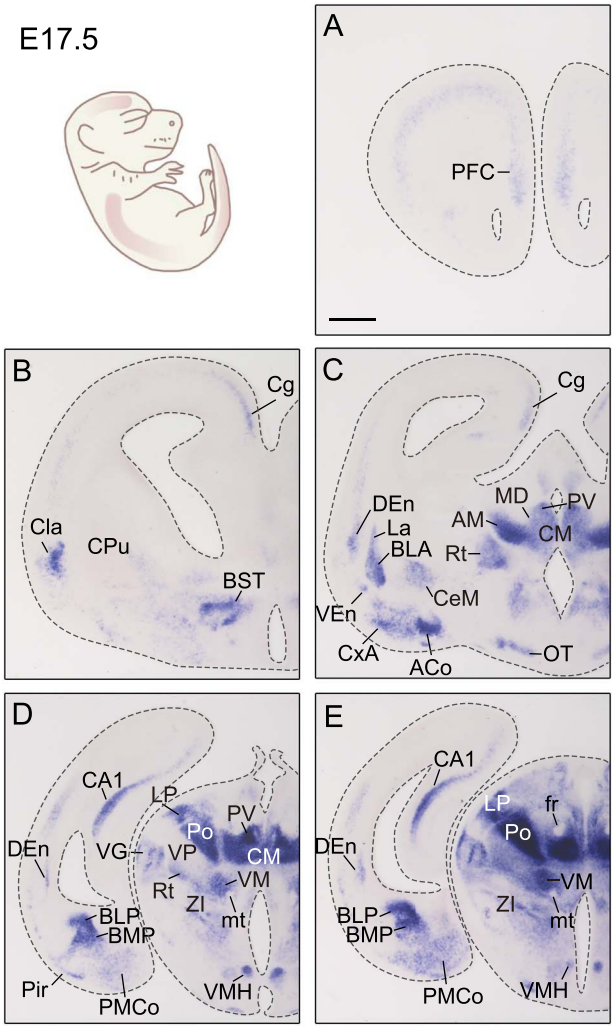

Figure 3. Embryonic *Grin3a* expression. (*A-E*) Representative images of colorimetric ISH showing *Grin3a* mRNA expression in E17.5 mouse embryos at various rostro-caudal levels. Abbreviations: ACo, anterior cortical amygdaloid nucleus; AM, anteromedial thalamic nucleus; BLA, basolateral amygdala, anterior part; BLP, basolateral amygdala, posterior part; BMP, basomedial amygdala, posterior part; BST, bed nucleus of the stria terminalis; CA1, Cornu Ammonis 1; CeM, central amygdaloid nucleus; Cg, cingulate cortex; Cla, claustrum; CM, centromedial thalamic nucleus; CPu, caudate-putamen; CxA, cortex amygdala transition zone; DEn, dorsal endopiriform nucleus; fr, fasciculus retroflexus; La, lateral amygdala; LP, lateral posterior thalamic nucleus; MD, medio dorsal thalamic nucleus; mt, mammillothalamic tract; OT, olfactory tubercle; PFC, prefrontal cortex; Pir, piriform cortex; PMCo, posteromedial cortical amygdaloid nucleus; Po, posterior thalamic nuclear group; PV, paraventricular nucleus; Rt, reticular thalamic nucleus; VEn, ventral endopiriform nucleus; VG, ventrolateral geniculate nucleus; VM, ventromedial thalamic nucleus; VMH, ventromedial hypothalamic nucleus; VP, ventroposterior thalamic nucleus; ZI, zona incerta. Scale bar: 500 µm.

and motor cortex and primary sensory cortices such as the somatosensory and auditory (Fig. 4*B, G, L, Q*). Expression in visual cortex was delayed and appeared around P6 (see Fig. 4*P-R*).

By P12, down-regulation had taken place in most regions and the characteristic adult pattern illustrated in Figure 1, with restriction to the amygdala, olfactory cortex, cortical amygdala, claustrum, and selected cortical and thalamic regions, was reached (Fig. 4*E, J, O, T*). Expression in CA1 became restricted to its ventral division (Figure 4*O, T*, see Supplementary Fig. 2).

Temporal Dynamics of Cortical *Grin3a* Expression Across Layers and Sensory Modalities

A major feature of developmental *Grin3a* expression in the neocortex was the initial predominance as an intense band in deeper cortical layers with later spread to other cortical laminae. To establish the laminar specificity of *Grin3a* expression, we combined fluorescence ISH with immunohistochemistry for the layer-specific markers Ctip2 and Cux1 that label pyramidal neurons in layer V and layers II–IV, respectively. Focused on P6 primary somatosensory cortex (SS1), we found that the highest number of *Grin3a*-positive fluorescent cells populate layer V as determined by colocalization with Ctip2 (Fig. 5A). A subset of layer V cells could be distinguished by their strong *Grin3a* mRNA labeling (Fig. 5B, bottom panel). Only a few *Grin3a*-positive cells with much lower fluorescence signal were detected in layers II/III (Fig. 5B, upper panel).

A finer temporal analysis covering earlier to late postnatal stages revealed a highly reproducible pattern of sequential *Grin3a* expression, which extends from deep to superficial layers, but which timing varied across sensory modalities. For instance: in SS1 *Grin3a* expression begins early in layer V, with *Grin3a*-positive cells already detected in newborns (P0). A gradual increase in the number of *Grin3a*-positive cells and *Grin3a* intensity levels in layer V was observed through P3–P6. Laminar specificity became less apparent at P9 and was lost by P12 (Fig. 5C, upper panels). Quantification of signal intensities across SS1 confirmed a sharp peak of *Grin3a* expression in layer V which reached a maximum at P6, and appearance of a second peak in layers II/III by P9 (Fig. 5D, upper graph). Expression in layer V declined significantly by P9-P12 (Fig. 5D, red vs. blue and green traces; see Supplementary Table 2). A comparison with primary visual cortex (V1) demonstrated a delayed onset of *Grin3a* expression relative to SS1 (Fig. 5C, bottom panels) or motor cortex (not shown). By P6 only a few, weakly labeled, *Grin3a*-positive cells were observed in layer V of V1 and expression peaked around P9–P12 (Fig. 5D, bottom graph). The spread to upper layers had not reached statistical significance by P12 and layer V down-regulation was also delayed relative to SS1 (blue vs. green lines in Fig. 5D, see Supplementary Table 2). The analysis demonstrates a precise laminar distribution of *Grin3a* expression, which changes over postnatal development and varies across sensory modalities, as exemplified by the shift in emergence and down-regulation between SS1 and V1.

Grin3a is Expressed in Excitatory and Inhibitory Neurons, with Predominance in Sst-Expressing Interneurons

We next aimed to achieve cellular resolution and define which neuronal subpopulations express *Grin3a*, focusing on SS1 cortex and dorsal hippocampus at P6–P9. The neocortex is composed of a majority of excitatory glutamatergic neurons (~80%) and a lower number of inhibitory GABAergic neurons (~20%). Thus, we conducted multiplex FISH assays using RNAscope probes for the vesicular glutamate transporter *vGlut1*, the GABA-synthesizing enzyme *Gad1* (glutamate decarboxylase 1), and *Grin3a* (Fig 6*A*). In SS1, *Grin3a* mRNA was expressed in both excitatory and inhibitory neurons as demonstrated by colocalization of

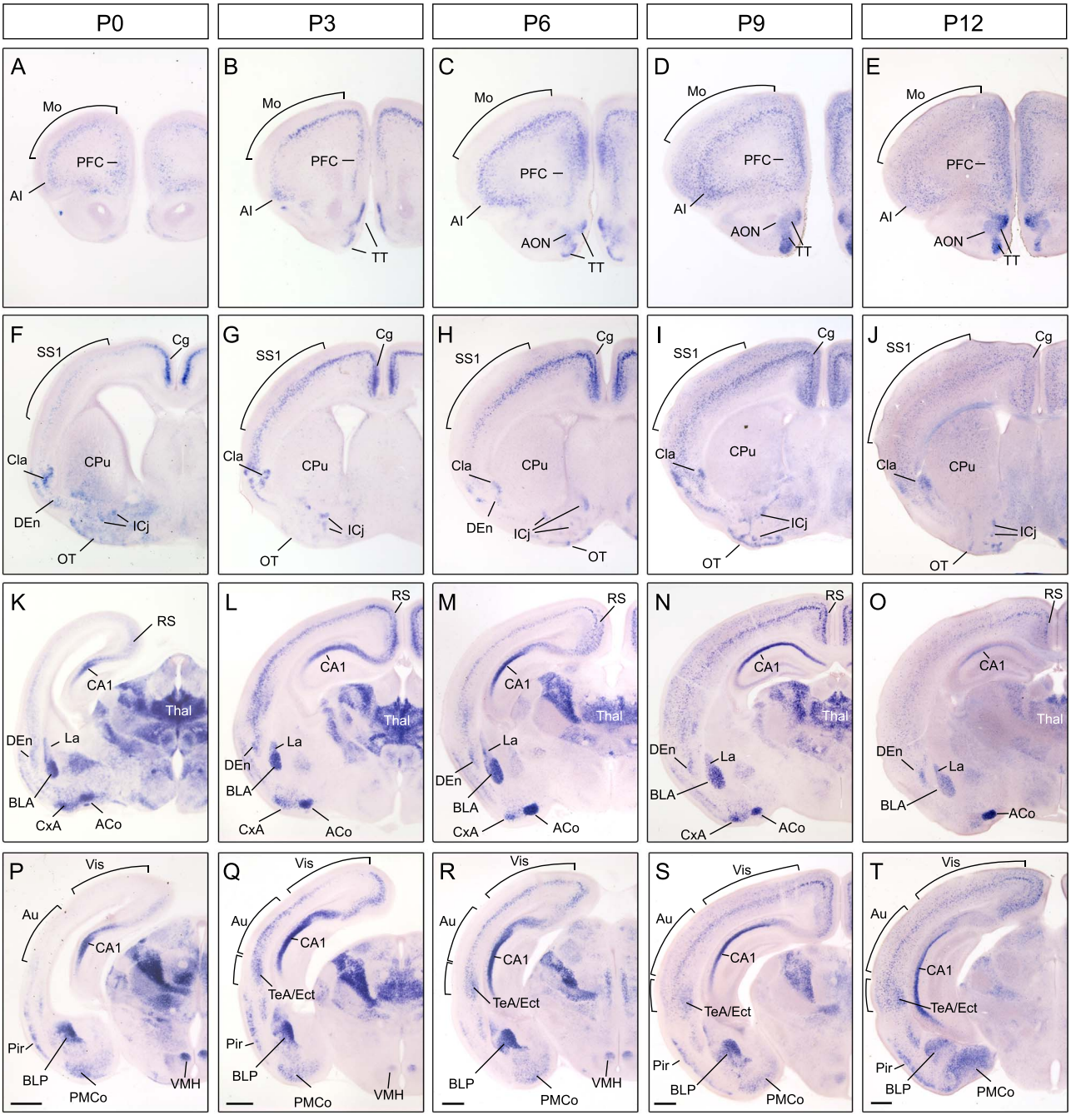

Figure 4. Emergence and down-regulation of *Grin3a* expression throughout postnatal developmental stages. (*A*-*T*) Colorimetric ISH for *Grin3a* mRNA in mouse brain at different postnatal (P) stages. Representative images of coronal sections at different rostro-caudal levels and indicated ages are shown. Abbreviations: ACo, anterior cortical amygdaloid nucleus; AI, agranular insular cortex; AON, anterior olfactory nucleus; Au, auditory cortex; BLA, basolateral amygdala; BLP, basolateral amygdaloid nucleus, posterior part; CA1, cornu ammonis 1; Cg, cingulate cortex; Cla, claustrum; CPu, caudate-putamen; CxA, cortex amygdala transition zone; DEn, dorsal endopiriform nucleus; Ect, ectorhinal cortex; ICj, islands of Calleja; La, lateral amygdaloid nucleus; Mo, motor cortex; PFC, prefrontal cortex; OT, olfactory tubercle; Pir, piriform cortex; PMCo, posteromedial cortical amygdaloid nucleus; RS, retrosplenial cortex; SS1, somatosensory cortex 1; TeA, temporal association cortex; Thal, thalamus; TT, tenia tecta; Vis, visual cortex; VMH, ventromedial hypothalamic nucleus. Scale bar: 500 µm.

punctate nuclear labeling with *vGlut1* or *Gad1* mRNA (Fig. 6*B*). Quantitatively, about half of *Grin3a*-positive neurons were *Gad1*-positive (51.57% ± 1.63) and the other half were *vGlut1*-positive (48.29% ± 1.66) (Fig. 6*D*). Strongest expression was typically found in GABAergic interneurons (Fig. 6*D*). In the hippocampus, a majority of CA1 pyramidal excitatory neurons expressed *Grin3a* (Fig. 6*C*). We additionally identified a subpopulation of inhibitory *Gad1*-positive neurons that displayed strong *Grin3a* labeling in the stratum oriens, whereas inhibitory interneurons intercalated in the CA1 pyramidal layer or in the stratum radiatum lacked *Grin3a* expression (Fig. 6*C*, *E*). Similar results were obtained when *Grin3a* localization in inhibitory interneurons was examined by conventional double FISH with riboprobes against *Grin3a* and *Gad1* (see Supplementary

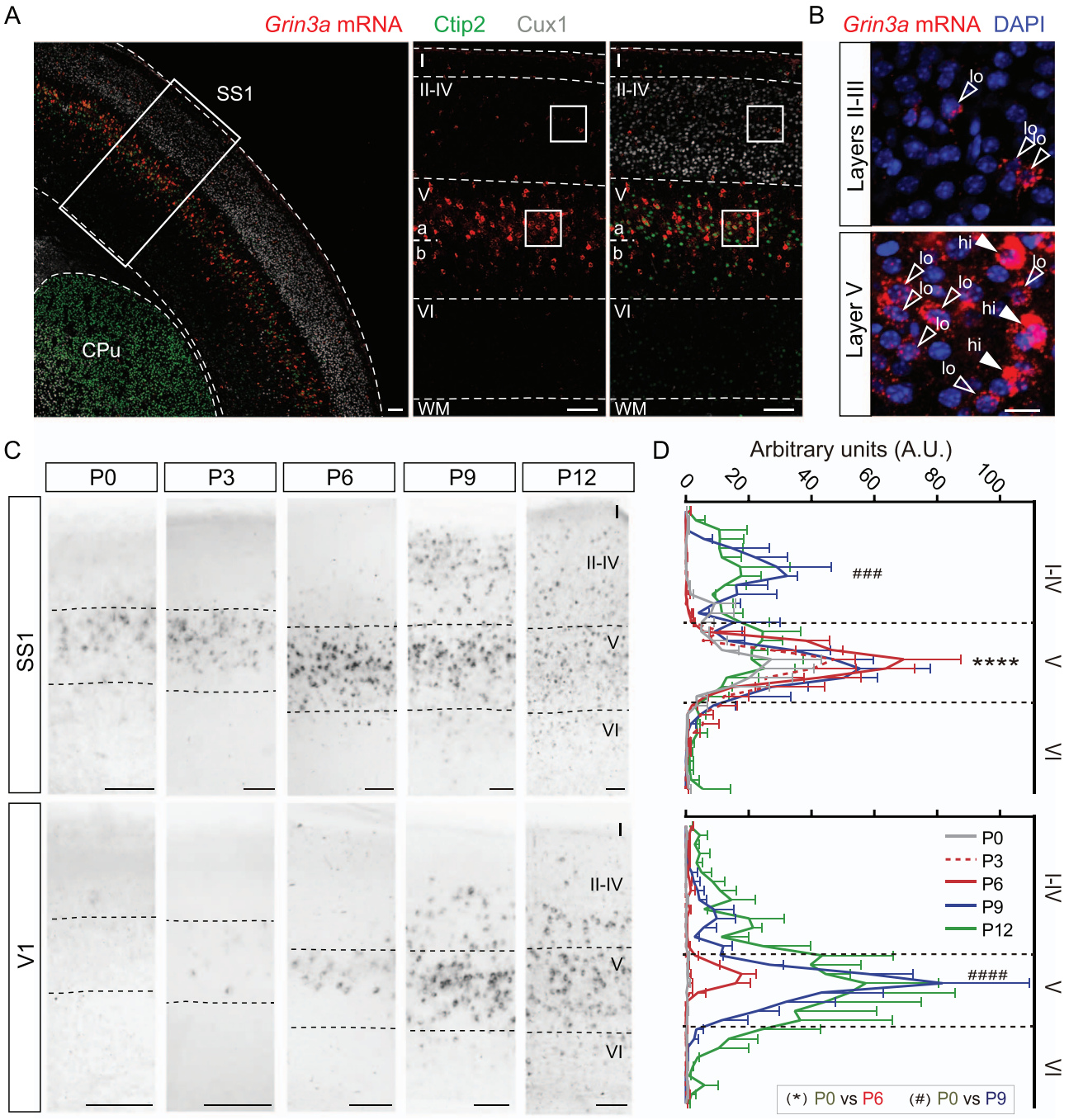

Figure 5. Dynamic temporal patterns of Grin3a expression across cortical layers and sensory modalities. (*A*) Left, mosaic of single confocal images of somatosensory cortex 1 (SS1) at P6 showing fluorescence ISH labeling of *Grin3a* mRNA (red) combined with immunofluorescence staining for Citp2 (green) and Cux1 (gray). Middle, right: higher magnification images of the boxed area on the left. Dotted lines mark boundaries between areas (left panel) or cortical layers (middle-right panels). (*B*) High-magnification images of boxed areas in layers II–III and V of the middle panel in A. *Grin3a* mRNA (red) and DAPI-stained nuclei (blue) are shown. Solid arrows indicate cells with high *Grin3a* mRNA levels; empty arrows show cells with low *Grin3a* mRNA levels. (*C*, *D*) Comparative analysis of the time-courses of *Grin3a* emergence and down-regulation in SS1 and primary visual cortex (V1). (*C*) Representative images show colorimetric ISH for *Grin3a* mRNA in SS1 and V1 at indicated postnatal ages. Dotted lines mark layer V boundaries. (*D*) Graphs of *Grin3a* mRNA intensity levels across layers in SS1 (top) and V1 (bottom) at P0 (gray), P3 (dashed red), P6 (red), P9 (blue), P12 (green). Data are mean ± S.E.M ($n = 3$ mice per postnatal age; 2 cortical fields taken at different levels were analyzed per mouse). Shown are statistical significances between P0 and P6 (****$P < 0.0001$) and between P0 and P9 ($^{###}P < 0.001$, $^{####}P < 0.0001$) calculated using two-way ANOVA followed by Bonferroni's multiple comparisons test. All others can be found in Supplementary Table 2. CPu, caudate-putamen; SS1, primary somatosensory cortex 1; V1, primary visual cortex 1. Scale bars: 100 µm (*A*), 20 µm (*B*), 100 µm (*C*).

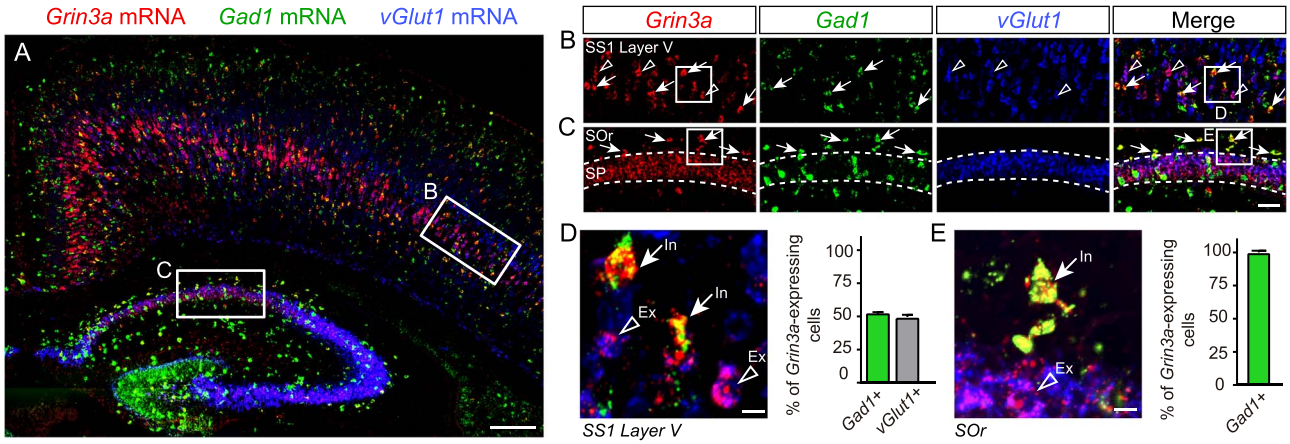

Figure 6. *Grin3a* expression in excitatory and inhibitory neurons. (*A*) Representative coronal section from a P6 wild-type mouse brain labeled by RNAscope for *Grin3a* mRNA (red) and markers of inhibitory (green: *Gad1* mRNA) and excitatory neurons (blue: *vGlut1* mRNA). (*B*, *C*) High-magnification images of the boxed areas in A corresponding to SS1 and CA1 hippocampal subfield. In (*C*), dotted lines mark the boundary between the different hippocampal layers. (*D*) Higher magnification of the boxed area in B and quantification of percentage of *Grin3a*-positive cells in SS1 layer V which express inhibitory or excitatory markers at P6–P9. (*E*) Higher magnification of the boxed area in C and quantification of percentage of *Grin3a* mRNA positive cells in the SOr of CA1 that colocalize with *Gad1*. Solid arrows: *Grin3a* inhibitory neurons as shown by colocalization with *Gad1* mRNA. Empty arrowheads: *Grin3a* excitatory neurons as shown by colocalization with *vGlut1* mRNA. Data are mean ± S.E.M ($n = 4$ animals, 6 SS1 fields, and 5 SOr of CA1 at different antero-posterior levels were analyzed). Ex, excitatory neurons; In, inhibitory neurons; SOr, stratum oriens; SP, stratum pyramidale. Scale bars: 100 µm (*A*); 25 µm (*B*-*C*); 5 µm (*D*-*E*).

Fig. 3A) or using GAD67^{GFP} mice (Tamamaki et al. 2003) (see Supplementary Fig. 3B, C).

The two most prevalent types of interneurons are fast-spiking parvalbumin-containing interneurons and low-threshold spiking Sst interneurons, which are generated in the medial ganglionic eminence (MGE) and account for ~70% of all interneurons (Tricoire et al. 2011; Lim et al. 2018). To determine which interneuron populations express *Grin3a*, we used *Nkx2–1-cre*:Ai9^{tdTomato} transgenic mice where the tdTomato signal is restricted to MGE-derived interneurons (Madisen et al. 2010) (Fig. 7A-C). Quantitatively, 52.14% ± 2.44 of *Grin3a*-expressing cells colocalized with *tdTomato* mRNA in SS1 layer V (Fig. 7D), a figure almost identical to the 51.57% of *Grin3a*-positive cells that colocalize with *Gad1* (Fig. 6D), indicating that essentially all *Grin3a*-expressing interneurons derive from MGE progenitors. Of these, the majority expressed *Sst* mRNA at high levels (34.88% ± 2.45 of the *Grin3a*-expressing population that is ~70% of all *Grin3a*-positive interneurons, Fig. 7D). At present, it is unclear if the remaining *tdTomato*-positive/*Sst*-negative cells belong to a population of immature Sst-fated interneurons that have not yet upregulated *Sst* mRNA levels, a different MGE-derived population such as parvalbumin cells, or a subset of MGE-derived cells that do not express either parvalbumin or Sst (Petros et al. 2015). Since parvalbumin is not upregulated in cortical interneurons until the second postnatal week, we are unable to directly address this. Similar results were obtained in the stratum oriens where virtually all *Grin3a*-expressing cells expressed *tdTomato* and *Sst* (Fig. 7E). Conversely, nearly all *Sst*-positive interneurons expressed *Grin3a* (96.39% ± 0.98 of the total *Sst* population in SS1 layer V, 91.98% ± 3.10 in stratum oriens, Fig. 7F).

Discussion

We provide a comprehensive description of *Grin3a* expression in the mouse brain from embryonic to postnatal and adult stages. Our results recapitulate and expand with anatomical detail the major postnatal down-regulation known *a priori*, and additionally reveal highly dynamic and differential *Grin3a* regulation across different brain regions. We further show that *Grin3a* is expressed in both excitatory and inhibitory neurons, and identify a previously underappreciated enrichment of *Grin3a* mRNA in Sst interneurons. The work provides a roadmap for dissecting the diverse functions attributed to GluN3A-NMDARs in brain physiology, behavior, and disease states.

During early postnatal life, neuronal circuits in the brain are massively remodeled by experience via long-lasting plasticity mechanisms that stabilize subsets of synapses but weaken or eliminate others (Katz and Shatz 1996). GluN3A-NMDARs have been proposed to control the timing and magnitude of this remodeling by limiting classical NMDAR signaling until the arrival of sensory experience, and/or fine-tuning synapse plasticity and maturation at later stages (Roberts et al. 2009; Fiuza et al. 2013; Perez-Otano et al. 2016). Our anatomical work lends support for this idea by showing early, sequential, and transient (or protracted) expression of *Grin3a* in cortical areas over postnatal development.

The variations in the timing of *Grin3a* expression and down-regulation across cortical regions correlate with differences in time-scales of cortical maturation (Guillery 2005) and degree of functional specialization (Wang 2020). For instance, transient waves of *Grin3a* expression are a characteristic of primary sensory cortices (see Figure 5), whereas expression appears early and is retained in association and multimodal areas. Primary sensory cortices provide modality-specific information, and early maturation guided by experience is needed to sculpt receptive fields and preserve the fidelity of the information. By contrast, associative and multimodal cortices play an integrative role, have long, protracted maturation periods, and maintain a potential for plastic responses that primary sensory areas lose early (Guillery 2005). Adult *Grin3a* expression was also observed in noncortical areas with strong plasticity needs into adulthood or a functional requirement for association of multiple inputs such are the olfactory system, the amygdala, or the claustrum (see Figure 1). Within primary sensory cortices,

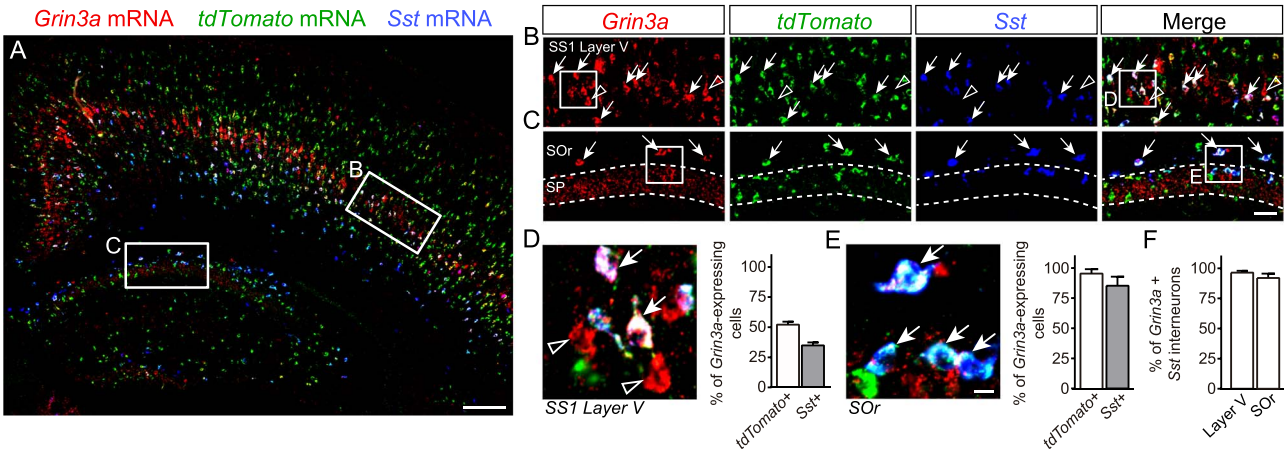

Figure 7. *Grin3a* expression in molecularly defined interneuron populations. RNAscope was used to assess colocalization of *Grin3a* and *Sst* mRNA in *Nkx2–1-cre*:Ai9^{tdTomato} mice that report MGE-derived interneurons. (*A*) Mosaic image of a P6 *Nkx2–1-cre*:Ai9^{tdTomato} mouse brain labeled for *Grin3a* mRNA (red) and specific cell-types (green: *tdTomato* mRNA; blue: *Sst* mRNA, somatostatin interneurons). Images of the corresponding boxes from SS1 (*B*) and CA1 area (*C*). Dotted lines mark the boundary between the different hippocampal layers. (*D*) Image of the boxed area in *B* (left panel) and quantification of *Grin3a*-positive cells that colocalize with *tdTomato* or *Sst* mRNA in SS1 layer V of P6–P9 mice (right panel). (*E*) Image of the boxed area in C (left panel) and quantification of *Grin3a*-positive cells that colocalize with *tdTomato* or *Sst* mRNA in the CA1 stratum oriens of P6–P9 mice (right panel). (*F*) Quantification of *Sst* mRNA positive cells that express *Grin3a* mRNA in SS1 layer V and stratum oriens. Solid arrows: *Grin3a* MGE-derived SSt interneurons as shown by colocalization with *tdTomato* and *Sst* mRNA. Empty arrowheads do not show colocalization and are likely *Grin3a*-positive excitatory neurons. Data are mean ± S.E.M ($n = 4$ animals, 5–6 fields at different rostro-caudal levels were analyzed). SOr, stratum oriens; SP, stratum pyramidale. Scale bars: 100 µm (*A*); 25 µm (*B-C*); 5 µm (*D-E*).

Grin3a expression follows a stereotyped sequential pattern with initial restriction to layer V followed by expression in outer layers and overall down-regulation (see Figure 5), which resembles the inside-out patterning model of cortical maturation. While this stereotyped pattern is conserved across motor and sensory cortices, its timing varies and is coupled to the arrival of sensory experience as exemplified by the delayed *Grin3a* expression in visual cortex, an area of the neocortex that matures later coinciding with eyelid opening (Yoshii et al. 2003).

Our findings confirm and expand a recent report that found *Grin3a* expression in adult mouse brain to be one of the strongest correlates with a hierarchical gradient of functional integration—from primary sensory to transmodal association cortices, established using the T1w/T2w magnetic resonance imaging ratio (Fulcher et al. 2019). In primate and mouse cortex, the T1w/T2w ratio inversely correlates with structural markers of increased differentiation and stability across cortices (Garcia–Cabezas et al. 2017; Wang 2020). Low T1w/T2w ratios and high *Grin3a* expression were found to be typical of functionally integrative areas in mouse and human brains (Fulcher et al. 2019), as also observed here. This is the case of the agranular cortex that receives not only sensory inputs but integrates multimodal information, or of the temporal association and rhinal cortices and the prefrontal cortex (Gogolla 2017). It is worth noting that genetic variations in human *GRIN3A* have been reported to modulate prefrontal cerebral activity during selective attention tasks (Gallinat et al. 2007), supporting a role in higher cognitive processing.

A number of parameters that vary over postnatal development and along the cortical hierarchy to fulfill specific functional requirements could be related to the *Grin3a* expression described here. For instance, GluN3A enhances spine turnover (Kehoe et al. 2014), and high rates of disassembly and formation of synapses and spines during postnatal critical periods are thought to be permissive for refinement while low spine turnover leads to circuit stabilization. GluN3A subunits have also been shown to control the developmental onset of long-term forms of plasticity such as hippocampal long-term potentiation (Roberts et al. 2009), spike-timing dependent long-term depression in V1 (Larsen et al. 2014), or the synaptic incorporation of GluN2A subunits and AMPA receptors (Henson et al. 2012). Other properties such as the maintenance of persistent or recurrent activity in the prefrontal cortex could reflect roles of GluN3A-NMDARs or excitatory GluN1/GluN3A receptors on NMDA spiking activity or neuronal excitability (Mahfooz et al. 2016; Otsu et al. 2019). Finally, association and frontal areas contain a greater proportion of Sst interneurons that innervate dendrites and have an "input-modulating function," while sensory areas contain more parvalbumin interneurons that innervate the soma and axon initial segment and have an "output-modulating" function.

Grin3a expression is very high in the thalamus where it prevails in higher order thalamic nucleus, while primary sensory thalamic areas lack *Grin3a* or express it at low levels. Information from the sensory periphery is first transmitted to the cerebral cortex via the primary sensory, or first-order, thalamic nuclei including the lateral geniculate in visual thalamus, ventral division of the medial geniculate in auditory thalamus, and ventral posterior nuclei in somatosensory thalamus. By contrast, higher order thalamic nuclei do not receive substantial input from the sensory periphery and instead form extensive cortico-thalamic-cortical circuits or connect functionally related cortical and subcortical regions. They provide a route for cortico-cortical communication which integrates cortical and subcortical inputs, linking cognition and motivated behavior to internal states and levels of consciousness (Sherman 2007). Of relevance here, highest adult *Grin3a* expression was observed in midline and intralaminar nuclei such as the centromedial and paraventricular, involved in arousal and wakefulness, and in the medial habenula, an epithalamic structure that controls negatively valued emotional associations (Van der Werf et al. 2002; Ren et al. 2018; Redinbaugh et al. 2020). Consistent with

these findings, unbiased mammalian reverse genetics detected alterations in wakefulness-sleep transitions in *Grin3a* knockout mice (Sunagawa et al. 2016), and GluN1/GluN3A glycine receptors in the medial habenula have been implicated in mediating conditioned place-aversion (Otsu et al. 2019).

Finally, our data revealed particularly high *Grin3a* mRNA levels in Sst interneurons of SS1 and hippocampus from early postnatal stages. This is in-line with single-cell RNAseq analyses of gene expression in adult mouse somatosensory and visual cortex interneurons (Pfeffer et al. 2013; Paul et al. 2017) (T Petros, et al, unpublished data). Publicly available transcriptome datasets indicate that *Grin3a* expression might be a conserved feature of Sst interneurons across species (http://interneuron.mccarrolllab.org/). Moreover, a recent genome-wide epigenomic analysis identified the *Grin3a* locus as a site of open chromatin and low DNA methylation (mCG) in Sst interneurons (Yao et al. 2020). Both epigenetic marks are typical of actively expressed genes and are thought to promote and maintain cell-type specific expression and cell identity.

Together these data provide strong validation of *Grin3a* expression as a secondary marker for Sst interneurons. They further suggest that GluN3A subunits might play more general roles than currently envisioned in modulating the development of neural circuits. Along with the well-studied refinements of connections between excitatory principal neurons, circuit formation requires the network integration of local interneurons that also involves a refinement of excitatory synaptic inputs onto these inhibitory cells (De Marco Garcia et al. 2015; Tuncdemir et al. 2016). For example, Sst interneurons in infragranular layers of SS1 receive dense but transient thalamocortical innervation during the first postnatal week. This innervation is required for the later functional maturation and synaptic integration of parvalbumin interneurons, but is reduced by 4-fold by P14 (Tuncdemir et al. 2016). Our data show that *Grin3a* is highly expressed between P3 and P9 in layer V Sst interneurons, providing a candidate mechanism for mediating the refinement of thalamocortical inputs. Excitatory synapses onto MGE-derived interneurons undergo a defined program of synapse maturation, with predominance of GluN2B-NMDARs in neonates which are later replaced by GluN2A-NMDARs (Matta et al. 2013; Perszyk et al. 2016). This developmental switch in subunit composition resembles the experienced by excitatory neurons, in which GluN3A down-regulation has been implicated (Perez-Otano and Ehlers 2004; Henson et al. 2012).

In sum, our study offers new insight onto the spatiotemporal patterns of *Grin3a* distribution in the brain and opens up important cell biological and functional questions. At the cell biological level, further investigations on regulation will be needed to define the transcriptional and epigenetic mechanisms that determine the area-to-area and temporal variations in *Grin3a* expression. Is experience a critical determinant factor, as suggested by the observation that rearing rats in the dark prevents GluN3A down-regulation in visual cortex (Larsen et al. 2014); or is regulation by the calcium-regulated transcription factor CaRF (Lyons et al. 2016)? In terms of function, the transient expression of *Grin3a* in cortical areas and temporal correlation with hierarchical cortical maturation emphasizes the concept of GluN3A as a key controller of the timing of brain maturation and its coupling to experience. Further advances will require selective deletion of the *Grin3a* gene at specific times and in specific neuronal populations, combined with tools to distinguish roles of GluN3A-NMDARs from those of the yet more enigmatic excitatory GluN1/GluN3 receptors.

Supplementary Material

Supplementary material can be found at *Cerebral Cortex* online.

Notes

We are grateful to Francisca Almagro-García for expert technical help, to Drs Francisco Clascá, Eloísa Herrera, Salvador Martínez, Elisa Mengual, John Wesseling, and Óscar Elía-Zudaire for advice on manuscript preparation, and Miguel Pérez-Otaño for help with graphic design.

We acknowledge support of the publication fee by the CSIC Open Access Publication Support Initiative through its Unit of Information Resources for Research (URICI). *Conflict of Interest:* None declared.

Funding

Spanish Ministry of Education and Science (BES-2014-069359 fellowship to A.M., SAF2016-80895-R grant to I.P.O., Severo-Ochoa Excellence Awards SEV-2013-0317 and SEV-2017-0723); the Generalitat Valenciana (PROMETEO 2019/020 grant to I.P.O); a NARSAD Independent Investigator Award (to I.P.O.); and NICHD Intramural Funding (to Y.Z. and T.J.P.).

References

Al-Hallaq RA, Jarabek BR, Fu Z, Vicini S, Wolfe BB, Yasuda RP. 2002. Association of NR3A with the N-methyl-D-aspartate receptor NR1 and NR2 subunits. *Mol Pharmacol*. 62:1119–1127.

Chatterton JE, Awobuluyi M, Premkumar LS, Takahashi H, Talantova M, Shin Y, Cui J, Tu S, Sevarino KA, Nakanishi N *et al*. 2002. Excitatory glycine receptors containing the NR3 family of NMDA receptor subunits. *Nature*. 415:793–798.

De Marco Garcia NV, Priya R, Tuncdemir SN, Fishell G, Karayannis T. 2015. Sensory inputs control the integration of neurogliaform interneurons into cortical circuits. *Nat Neurosci*. 18:393–401.

Eriksson M, Nilsson A, Froelich-Fabre S, Akesson E, Dunker J, Seiger A, Folkesson R, Benedikz E, Sundstrom E. 2002. Cloning and expression of the human N-methyl-D-aspartate receptor subunit NR3A. *Neurosci Lett*. 321:177–181.

Fiuza M, Gonzalez-Gonzalez I, Perez-Otano I. 2013. GluN3A expression restricts spine maturation via inhibition of GIT1/Rac1 signaling. *Proc Natl Acad Sci USA*. 110:20807–20812.

Fulcher BD, Murray JD, Zerbi V, Wang XJ. 2019. Multimodal gradients across mouse cortex. *Proc Natl Acad Sci USA*. 116:4689–4695.

Gallinat J, Gotz T, Kalus P, Bajbouj M, Sander T, Winterer G. 2007. Genetic variations of the NR3A subunit of the NMDA receptor modulate prefrontal cerebral activity in humans. *J Cogn Neurosci*. 19:59–68.

Garcia-Cabezas MA, Joyce MKP, John YJ, Zikopoulos B, Barbas H. 2017. Mirror trends of plasticity and stability indicators in primate prefrontal cortex. *Eur J Neurosci*. 46:2392–2405.

Gogolla N. 2017. The insular cortex. *Curr Biol*. 27:R580–R586.

Grand T, Abi Gerges S, David M, Diana MA, Paoletti P. 2018. Unmasking GluN1/GluN3A excitatory glycine NMDA receptors. *Nat Commun*. 9:4769.

Guillery RW. 2005. Is postnatal neocortical maturation hierarchical? *Trends Neurosci*. 28:512–517.

Harris JA, Mihalas S, Hirokawa KE, Whitesell JD, Choi H, Bernard A, Bohn P, Caldejon S, Casal L, Cho A *et al*. 2019. Hierarchical

organization of cortical and thalamic connectivity. *Nature*. 575:195–202.

Henson MA, Larsen RS, Lawson SN, Perez-Otano I, Nakanishi N, Lipton SA, Philpot BD. 2012. Genetic deletion of NR3A accelerates glutamatergic synapse maturation. *PLoS One*. 7:e42327.

Huang X, Chen YY, Shen Y, Cao X, Li A, Liu Q, Li Z, Zhang LB, Dai W, Tan T *et al*. 2017. Methamphetamine abuse impairs motor cortical plasticity and function. *Mol Psychiatry*. 22:1274–1281.

Katz LC, Shatz CJ. 1996. Synaptic activity and the construction of cortical circuits. *Science*. 274:1133–1138.

Kehoe LA, Bellone C, De Roo M, Zandueta A, Dey PN, Perez-Otano I, Muller D. 2014. GluN3A promotes dendritic spine pruning and destabilization during postnatal development. *J Neurosci*. 34:9213–9221.

Kim J, Matney CJ, Roth RH, Brown SP. 2016. Synaptic organization of the neuronal circuits of the claustrum. *J Neurosci*. 36:773–784.

Larsen RS, Smith IT, Miriyala J, Han JE, Corlew RJ, Smith SL, Philpot BD. 2014. Synapse-specific control of experience-dependent plasticity by presynaptic NMDA receptors. *Neuron*. 83:879–893.

Lee JH, Wei L, Deveau TC, Gu X, Yu SP. 2016. Expression of the NMDA receptor subunit GluN3A (NR3A) in the olfactory system and its regulatory role on olfaction in the adult mouse. *Brain Struct Funct*. 221:3259–3273.

Lim L, Mi D, Llorca A, Marin O. 2018. Development and functional diversification of cortical interneurons. *Neuron*. 100:294–313.

Lyons MR, Chen LF, Deng JV, Finn C, Pfenning AR, Sabhlok A, Wilson KM, West AE. 2016. The transcription factor calcium-response factor limits NMDA receptor-dependent transcription in the developing brain. *J Neurochem*. 137:164–176.

Madisen L, Zwingman TA, Sunkin SM, Oh SW, Zariwala HA, Gu H, Ng LL, Palmiter RD, Hawrylycz MJ, Jones AR *et al*. 2010. A robust and high-throughput Cre reporting and characterization system for the whole mouse brain. *Nat Neurosci*. 13:133–140.

Mahfooz K, Marco S, Martinez-Turrillas R, Raja MK, Perez-Otano I, Wesseling JF. 2016. GluN3A promotes NMDA spiking by enhancing synaptic transmission in Huntington's disease models. *Neurobiol Dis*. 93:47–56.

Marco S, Giralt A, Petrovic MM, Pouladi MA, Martinez-Turrillas R, Martinez-Hernandez J, Kaltenbach LS, Torres-Peraza J, Graham RK, Watanabe M *et al*. 2013. Suppressing aberrant GluN3A expression rescues synaptic and behavioral impairments in Huntington's disease models. *Nat Med*. 19:1030–1038.

Marco S, Murillo A, Perez-Otano I. 2018. RNAi-based GluN3A silencing prevents and reverses disease phenotypes induced by mutant Huntington. *Mol Ther*. 26:1965–1972.

Matta JA, Pelkey KA, Craig MT, Chittajallu R, Jeffries BW, McBain CJ. 2013. Developmental origin dictates interneuron AMPA and NMDA receptor subunit composition and plasticity. *Nat Neurosci*. 16:1032–1041.

Mohamad O, Song M, Wei L, Yu SP. 2013. Regulatory roles of the NMDA receptor GluN3A subunit in locomotion, pain perception and cognitive functions in adult mice. *J Physiol*. 591:149–168.

Mueller HT, Meador-Woodruff JH. 2003. Expression of the NR3A subunit of the NMDA receptor in human fetal brain. *Ann N Y Acad Sci*. 1003:448–451.

Mueller HT, Meador-Woodruff JH. 2004. NR3A NMDA receptor subunit mRNA expression in schizophrenia, depression and bipolar disorder. *Schizophr Res*. 71:361–370.

Otsu Y, Darcq E, Pietrajtis K, Matyas F, Schwartz E, Bessaih T, Abi Gerges S, Rousseau CV, Grand T, Dieudonne S *et al*. 2019. Control of aversion by glycine-gated GluN1/GluN3A NMDA receptors in the adult medial habenula. *Science*. 366:250–254.

Pachernegg S, Strutz-Seebohm N, Hollmann M. 2012. GluN3 subunit-containing NMDA receptors: not just one-trick ponies. *Trends Neurosci*. 35:240–249.

Paoletti P, Bellone C, Zhou Q. 2013. NMDA receptor subunit diversity: impact on receptor properties, synaptic plasticity and disease. *Nat Rev Neurosci*. 14:383–400.

Paul A, Crow M, Raudales R, He M, Gillis J, Huang ZJ. 2017. Transcriptional architecture of synaptic communication delineates GABAergic neuron identity. *Cell*. 171:522, e520–539.

Paxinos G, Franklin K. 2019. *Mouse brain in stereotaxic coordinates*. 5th ed. Amsterdam (Netherlands): Academic Press.

Paxinos G, Halliday G, Watson C, Koutcherov Y, Wang H. 2007. *Atlas of the developing mouse brain*. 1st ed. Amsterdam (Netherlands): Academic Press.

Perez-Otano I, Ehlers MD. 2004. Learning from NMDA receptor trafficking: clues to the development and maturation of glutamatergic synapses. *Neurosignals*. 13:175–189.

Perez-Otano I, Larsen RS, Wesseling JF. 2016. Emerging roles of GluN3-containing NMDA receptors in the CNS. *Nat Rev Neurosci*. 17:623–635.

Perez-Otano I, Schulteis CT, Contractor A, Lipton SA, Trimmer JS, Sucher NJ, Heinemann SF. 2001. Assembly with the NR1 subunit is required for surface expression of NR3A-containing NMDA receptors. *J Neurosci*. 21:1228–1237.

Perszyk RE, DiRaddo JO, Strong KL, Low CM, Ogden KK, Khatri A, Vargish GA, Pelkey KA, Tricoire L, Liotta DC *et al*. 2016. GluN2D-containing N-methyl-d-aspartate receptors mediate synaptic transmission in hippocampal interneurons and regulate interneuron activity. *Mol Pharmacol*. 90:689–702.

Petros TJ, Bultje RS, Ross ME, Fishell G, Anderson SA. 2015. Apical versus basal neurogenesis directs cortical interneuron subclass fate. *Cell Rep*. 13:1090–1095.

Pfeffer CK, Xue M, He M, Huang ZJ, Scanziani M. 2013. Inhibition of inhibition in visual cortex: the logic of connections between molecularly distinct interneurons. *Nat Neurosci*. 16:1068–1076.

Redinbaugh MJ, Phillips JM, Kambi NA, Mohanta S, Andryk S, Dooley GL, Afrasiabi M, Raz A, Saalmann YB. 2020. Thalamus modulates consciousness via layer-specific control of cortex. *Neuron*. 106:66, e12–75.

Ren S, Wang Y, Yue F, Cheng X, Dang R, Qiao Q, Sun X, Li X, Jiang Q, Yao J *et al*. 2018. The paraventricular thalamus is a critical thalamic area for wakefulness. *Science*. 362:429–434.

Roberts AC, Diez-Garcia J, Rodriguiz RM, Lopez IP, Lujan R, Martinez-Turrillas R, Pico E, Henson MA, Bernardo DR, Jarrett TM *et al*. 2009. Downregulation of NR3A-containing NMDARs is required for synapse maturation and memory consolidation. *Neuron*. 63:342–356.

Sherman SM. 2007. The thalamus is more than just a relay. *Curr Opin Neurobiol*. 17:417–422.

Sucher NJ, Akbarian S, Chi CL, Leclerc CL, Awobuluyi M, Deitcher DL, Wu MK, Yuan JP, Jones EG, Lipton SA. 1995. Developmental and regional expression pattern of a novel NMDA receptor- like subunit (NMDAR-L) in the rodent brain. *J Neurosci*. 15:6509–6520.

Sunagawa GA, Sumiyama K, Ukai-Tadenuma M, Perrin D, Fujishima H, Ukai H, Nishimura O, Shi S, Ohno RI, Narumi

R *et al*. 2016. Mammalian reverse genetics without crossing reveals Nr3a as a short-sleeper gene. *Cell reports*. 14:662–677.

Tamamaki N, Yanagawa Y, Tomioka R, Miyazaki J, Obata K, Kaneko T. 2003. Green fluorescent protein expression and colocalization with calretinin, parvalbumin, and somatostatin in the GAD67-GFP knock-in mouse. *J Comp Neurol*. 467:60–79.

Tricoire L, Pelkey KA, Erkkila BE, Jeffries BW, Yuan X, McBain CJ. 2011. A blueprint for the spatiotemporal origins of mouse hippocampal interneuron diversity. *J Neurosci*. 31: 10948–10970.

Tuncdemir SN, Wamsley B, Stam FJ, Osakada F, Goulding M, Callaway EM, Rudy B, Fishell G. 2016. Early Somatostatin interneuron connectivity mediates the maturation of deep layer cortical circuits. *Neuron*. 89:521–535.

Van der Werf YD, Witter MP, Groenewegen HJ. 2002. The intralaminar and midline nuclei of the thalamus. Anatomical and functional evidence for participation in processes of arousal and awareness. *Brain Res Brain Res Rev*. 39:107–140.

Wang XJ. 2020. Macroscopic gradients of synaptic excitation and inhibition in the neocortex. *Nat Rev Neurosci*. 21:169–178.

Watson C, Paxinos G, Puelles L. 2012. *Mouse nervous system*. 1st ed. Amsterdam (Netherlands): Academic Press.

Wong HK, Liu XB, Matos MF, Chan SF, Perez-Otano I, Boysen M, Cui J, Nakanishi N, Trimmer JS, Jones EG *et al*. 2002. Temporal and regional expression of NMDA receptor subunit NR3A in the mammalian brain. *J Comp Neurol*. 450:303–317.

Xu Q, Tam M, Anderson SA. 2008. Fate mapping Nkx2.1-lineage cells in the mouse telencephalon. *J Comp Neurol*. 506: 16–29.

Yang J, Wang S, Yang Z, Hodgkinson CA, Iarikova P, Ma JZ, Payne TJ, Goldman D, Li MD. 2015. The contribution of rare and common variants in 30 genes to risk nicotine dependence. *Mol Psychiatry*. 20:1467–1478.

Yao Z, Liu H, Xie F, Fischer S, Booeshaghi AS, Adkins RS, Aldridge AI, Ament SA, Pinto-Duarte A, Bartlett A *et al*. 2020. An integrated transcriptomic and epigenomic atlas of mouse primary motor cortex cell types. *bioRxiv*. doi: https://doi.org/10.1101/2020.02.29.970558.

Yoshii A, Sheng MH, Constantine-Paton M. 2003. Eye opening induces a rapid dendritic localization of PSD-95 in central visual neurons. *Proc Natl Acad Sci USA*. 100:1334–1339.

Yuan T, Mameli M, EC OC, Dey PN, Verpelli C, Sala C, Perez-Otano I, Luscher C, Bellone C. 2013. Expression of cocaine-evoked synaptic plasticity by GluN3A-containing NMDA receptors. *Neuron*. 80:1025–1038.